Local and trans-oceanic tsunamis in the Bering and Chukchi seas based on numerical modeling

Alisa Medvedeva (Alisa.bannikova@gmail.ru)
Shirshov Institute of Oceanology RAS
Igor Medvedev
Shirshov Institute of Oceanology RAS
Isaac Fine
Institute of Ocean Sciences, Sidney, BC
Evgueni Kulikov
Shirshov Institute of Oceanology RAS
Olga Yakovenko
Shirshov Institute of Oceanology RAS

Research Article

Keywords: Bering Sea, Chukchi Sea, Arctic, tsunami, Pacific Ocean, earthquake, trans-oceanic tsunami, distant earthquake, Chilean earthquake, tsunami source, Aleutian Islands, seismic source, tsunami modeling

Posted Date: August 22nd, 2022

DOI: https://doi.org/10.21203/rs.3.rs-1932671/v1

Additional Declarations: No competing interests reported.

Version of Record: A version of this preprint was published at Pure and Applied Geophysics on April 5th, 2023. See the published version at https://doi.org/10.1007/s00024-023-03251-9.

Abstract

We have examined the tsunami risk in the Bering and Chukchi seas by determining whether trans-oceanic tsunamis penetrate into these regions through the Aleutian Islands and Bering Strait. Results are based on numerical modeling of eight major far-field earthquakes in the North Pacific Ocean and one near-field earthquake that occurred in the Bering Sea region: the 1946 Aleutian, 1952 Kamchatka, 1960 Chile, 1964 Alaska, 1965 Rat Islands, 1957 Andreanof Islands, 2011 Tohoku, 2012 Haida Gwaii, and 2017 Commander Islands earthquakes. It was found that the most powerful event to impact the Bering Sea was the 1960 tsunami generated by the M_W 9.5 Chilean earthquake. According to our numerical simulations, the 1960 earthquake produced tsunami waves with amplitudes up to 192 cm in the sea, while for the next strongest event, the 1952 Kamchatka tsunami, the wave amplitudes were up to 177 cm. The 1964 Great Alaska earthquake (M_W 9.2) did not produce an intense tsunami in the Bering Sea because the lone and narrow southwestern extension of the Alaska Peninsula sheltered the region from incoming tsunami waves. Modeling further shows that, in separate bays, tsunami waves formed by strong distant earthquakes could reach 1—1.5 m. Results show that the typical attenuation coefficient for the straits of the Aleutian Islands is 0.75, on average, while the corresponding coefficient upon transition from the Bering Sea to the Chukchi Sea through the Bering Strait is ~ 0.25. Based on these estimates, we conclude that tsunami penetration into the Arctic Ocean from remote sources in the Pacific is unlikely. Even for such powerful events as the 1960 Chilean tsunami, the tsunami wave amplitudes in the Chukchi Sea would not exceed a few centimeters.

1. Introduction

Tsunami hazards for the Arctic region including the Bering and Chukchi seas are traditionally considered as insignificant due to the low seismic activity in the region. Low population density and rare tide gauge network lead to the lack of information on tsunami hazards here. Nowadays, approximately 33 500 people live on the Russian coast of the Bering Sea and about 8500 people on the coast of the Chukchi Sea; roughly 23 500 people live on the American coast of the Bering Sea and about 11 200 people - on the islands of these two seas. At the same time, the catastrophic tsunamis of the last two decades, namely the 2004 Sumatra, 2010 Chile, and 2011 Tohoku events, as well as two recent 2018 tsunamis in Indonesia (Sulawesi and Anak-Krakatau), demonstrate the serious threats of major seismically generated tsunamis in various regions of the World Ocean, even in those, where tsunami waves have never been observed before. The Arctic is becoming more important because of increasing economic activity and due to the climate and geopolitical changes. Therefore, it is natural to ask: *What is the tsunami hazard at the coast of the Bering Sea and within the entire Arctic Region?* Unfortunately, due to the lack of necessary information, the problem of tsunami hazard for the coasts of the Bering and Chukchi seas is highly relevant and requires detailed studies. The paleotsunami studies conducted in this region (Bourgeois et al., 2006; Gordeev et al., 2015; Pinegina, 2018; Pinegina et al., 2020) demonstrate that significant tsunamis have occurred in this region in the past, and, therefore, can occur in the future.

A history of tsunamis along the Bering coast of the Kamchatka region over the past 4000 years indicates that the northern Kuril-Kamchatka Subduction Zone produces tsunamigenic earthquakes every few centuries (Bourgeois et al., 2006). That zone and the zone along the west margin of the Bering Sea are the main

tsunamigenic regions. The most powerful known earthquakes in this area were the 1969 M_w 7.4 earthquake near the Ozernoi Peninsula (Pinegina et al., 2014), the 1991 Khailinskoe (M_w 6.6), and the 2006 Olytorskoe (M_w 7.6) earthquakes. Analysing the 4500-year paleoseismic record, Pinegina et al. (2014) documented 12–15 tsunamis in the southwestern part of the Bering Sea. The runups of those tsunamis were estimated to be up to 4–8 m with the inland inundation was ~ 300–400 m. Therefore, the authors assumed that those waves were produced by local earthquakes with M_w 7.5 ± 0.5. As for the west and northwest coasts of the Bering Sea, the slip along faults, deforming the late Pleistocene-Holocene marine terraces could be the main source of tsunamigenic earthquakes. The recurrence interval of a tsunami with the runup of > 5 m at various parts of the Bering Sea coast varies from 125 to 1000 years (Pinegina et al., 2014).

Newly compiled Russian and U.S. seismological data, according to Mackey et al. (1997) shows an independent Bering block motion relative to the North American Plate. The Bering block includes most of the Bering Sea, the Chukchi Peninsula, the Seward Peninsula and parts of western Alaska. This motion is probably driven by the westward extrusion of southwestern Alaska resulting from the compression in southern Alaska due to the subduction of the Pacific Plate and terrane accretion. The seismicity spreads from central Alaska through the Bering Strait into the Chukotka Peninsula. In the eastern Chukotka region several southwest trends are evident, some of which continue to pass on through the Koryak Highlands to Kamchatka. The focal mechanisms, young basaltic volcanism and normal faults in western Alaska and Chukotka indicate that the Bering Strait is under the northeast-southwest extension. This, in conjunction with the thrust faulting in the Koryak Highlands, indicates that the Bering block rotates clockwisely relative to the North American Plate (Mackey et al., 1997). According to the United States Geological Survey (USGS) catalog, one of the strongest earthquakes in the Chukchi Sea was on 21 February 1928, with a magnitude M_w 6.6. In the central part of the Bering Sea, an earthquake with a magnitude of 6.5 occurred on 26 February 1928.

The synthetic catalog of earthquakes within the Arctic region was created by Kulikov et al. (2019a). According to that catalog, the mean recurrence period of earthquakes with $M_w \geq 7$ for the Chukchi Sea and Bering Strait was about 450 years, and about 5000 years for the events with $M_w \geq 7.5$. Based on this catalog, Kulikov et al. (2019b) reconstructed the tsunami sources and estimated probabilistic characteristics of tsunami hazards on the Arctic coast of the Russian Federation with the help of the catalog. The maximum tsunami height with a recurrence period of 1000 years for the Chukchi Sea and the Bering Strait was less than 0.2 m.

It is well known, that major earthquakes can generate trans-oceanic tsunamis that can destructively spread over great distances (Gusiakov, 2019). The strongest instrumentally recorded earthquake (M_w 9.5) occurred on 22 May 1960 near the coast of Chile. It generated one of the most destructive trans-Pacific tsunamis that were measured by about 200 tide gauges in the Pacific Ocean (Berkman & Symons, 1960), including far-field sites at the Aleutian Islands and in the Sea of Okhotsk located 13 000–16 000 kilometers from the source area. Berkman and Symons (1960) also pointed out that this tsunami was recorded at Fremantle and Port MacDonnell at the western coast of Australia, i.e. in the Indian Ocean. Evidence that the 1960 Chilean tsunami was a global-scale event was provided 27 years later, when Van Dorn (1987) examined British and other hydrographic archives and found six more records of this tsunami at certain sites in the Indian and

Atlantic oceans, including Bunbury (Western Australia), Mossel Bay, and Luderitz (South Africa); Mauritius Island (Indian Ocean), Bermuda Islands (Northwest Atlantic Ocean) and even Newlyn (United Kingdom).

Did the tsunamis reach the Bering and Chukchi Seas? What was their height there? How did the Aleutian Islands influence the penetration of great tsunamis into the Bering Sea? All the questions are considered in this study. Dudley and Lee (1998) noted that on 23 May 1960 the tsunami wave caused by this earthquake was observed in the Chukchi Sea at Point Hope (northwestern coast of Alaska). Lander (1996) noted: "*Eskimos on ice near Point Hope returned to shore when they heard the ice cracking in the afternoon. If this event was caused by the Chilean tsunami it would have had to travel under the still-frozen ice to reach and crack the thinner coastal ice as its amplitude increased in the shallower water. It could not have been caused by the seismic wave, which would have arrived within minutes of the origin time*." However, the wave height is not indicated in this catalog. There are a few more observations of the historical tsunamis at the coast of Bering Sea provided mostly by witness reports, therefore credibility of such reports is questionable. The instrumental records of tsunamis in the Bering Sea are associated with the 2011 Tohoku earthquake. A tide gauge at Saint Paul Island recorded a 61- cm wave, while the wave recorded at Nome (Alaska) was of only 4 cm (NGDC/WDS, 2022).

Because of lack of proper tsunami observations, the numerical modeling modeling allows to estimate tsunami risk in the area. The main purpose of the present study is to numerically simulate and evaluate expected wave heights in the Bering and Chukchi Seas produced by major trans-oceanic and local tsunamis. Specific attention is paid to the estimation of the Aleutian Islands and Bering Strait influence on attenuation of tsunami waves penetrating from the Pacific Ocean into the Bering Sea and then into the Arctic Ocean.

2. Data And Methods

We have studied the tsunami waves propagation using a numerical tsunami model (Fine et al., 2013), similar to TUNAMI (Imamura, 1996). It is based on the shallow water finite-difference equations. A linearized version of the shallow water equations was used. The corresponding numerical finite-difference approximation is conservative. While this linearization somewhat limits the accuracy of the model for coastal zones, it allows performing long-term simulations of the wave field, for which nonlinear effects are less important, and allows to control better the energy dissipation in the model. This model was configured for the Pacific Ocean and the adjacent part of the Arctic Ocean (80°S–80°N, 120°E–70°W; Fig. 1). It uses spherical coordinates with a grid size of 2 arc minutes and a time step of 2 seconds. The seafloor topographic grid was derived from the GEBCO 2014 database.

We considered the following nine tsunami events listed chronologically:

1. M_w = 8.6 – Aleutian Islands, USA, 01 April 1946;
2. M_w = 9.0 – Kamchatka, USSR, 4 November 1952;
3. $M_w \approx$ 8.6 – Andreanof Islands, USA, 9 March 1957;
4. M_w = 9.5 – Chile, 22 May 1960;
5. M_w = 9.2 – Alaska, USA, 27 March 1964;

6. M_w = 8.7 – Rat Islands, USA, 4 February 1965;
7. M_w = 9.0 – Tohoku, Japan, 11 March 2011;
8. M_w = 7.8 – Haida Gwaii, Canada, 28 October 2012;
9. $M_w \approx 7.7$ – Commander Islands, Russian Federation, 17 July 2017.

Our numerical study was mostly based a) on published tsunami sources (i.e., on distribution of the seabed displacements) or b) on published seismic sources. In both cases, the sources were already validated on tsunami observations using numerical models. However, we additionally used 3D elastic formulas (Okada, 1985) while working with the b) sources in order to reconstruct the distribution of the bottom displacement. In case when the seismic source contains several subfaults, the elastic formulas were applied to each subfault separately; the distribution of the bottom displacement accumulated the displacements from individual subfaults. The only case when the tsunami was not modeled before is if the tsunami generated by a recent earthquake at the Commander Islands in 2017.We used a USGS seismic moment solution to simulate this case. Nine input parameters were required to create seabed displacement by the Okada equations: two geographical coordinates, hypocenter depth, width and length of the fracture region, strike angle (*Strike*, °), dip angle (*Dip*, °), slip angle (*Rake*, °), and a displacement along the plane (slip value, *Slip*, m). From these parameters, the width, length and slip are unknown (though their product is related to the known seismic moment), therefore they were estimated via empirical scaling law (Wells and Coppersmith, 1994). The main parameters and types of used seismic sources are summarized in Table 1.

3. Results

Table 1
The principal information about nine earthquakes that were used in our numerical modeling of tsunami waves in the Bering and Chukchi seas.

№	Earthquake	M_W	Date	Lat.	Lon.	Depth (km)	Type of source	Reference
1	Aleutian Islands	8.6	01.04.1946	53.49°N	162.832°W	15	Subfaults[1]	Johnson and Satake, 1997
2	Kamchatka	9	04.11.1952	52.62°N	159.78°E	22	Subfaults[1]	Johnson and Satake, 1999
3	Andreanof Islands	8.6	09.03.1957	51.5°N	175.63°W	25	Subfaults[1]	Johnson et al., 1994
4	Chile	9.5	22.05.1960	38.14°S	73.41°W	30	Seafloor displacement	Moreno et al., 2009
5	Alaska	9.2	27.03.1964	60.91°N	147.34°W	25	Seafloor displacement	Suleimani et al., 2020
6	Rat Islands	8.7	04.02.1965	51.25°N	178.72°E	30	Subfaults[1]	Johnson and Satake, 1996
7	Tohoku-Oki	9.1	11.03.2011	38.3°N	142.37°E	29	Seafloor displacement	Hayes, 2011
8	Haida Gwaii	7.8	28.10.2012	52.79°N	132.1°W	14	Seafloor displacement	Fine et al., 2015
9	Commander Islands	7.7	17.07.2017	54.44°N	168.86°E	10	Single fault	USGS

[1]The seismic model was created using inverse tsunami modeling.

I. 1946 Aleutian. The Aleutian earthquake M_W=8.6 of 1 April 1946 is believed to be one of the most unusual seismic events of the 20th century. This earthquake generated a very strong trans-Pacific tsunami that hit the coast of Alaska, the Aleutian Islands, Hawaii, North and South America, killed 126 people and seriously damaged Hilo (Hawaii). The maximum runup height (35 m) was recorded near the source at Unimak Island lighthouse (Lander, 1996). The earthquake had moderate surface wave magnitude (M_S=7.4), so the generated tsunami was disproportionally large. That is why the earthquake was identified as the “tsunami earthquake”; the event attracted researchers for many years (e.g. Okal et al., 2003; Lopez et al., 2006; Rabinovich et al., 2019).

We used the seismic source based on the inversion of the tsunami waveform provided by (Jonhson and Satake, 1997). The preferable solution (Model B) consisted of three subfaults. Jonhson and Satake sought an optimal distribution of the slips on 3 subfaults on the plane with *strike* 250°, *dip* 6° and found out that the trust faults (*rake* 90°) at 9.8–9.6 m *slip* values provided considerable synthetic tsunami wave forms at most of tide gauge location at Alaska, Hawaii and California. The tsunami was generated by both vertical and horizontal displacements of the seabed. Figure 2a shows the results of the modeling of the 1946 Alaska tsunami in the Bering Sea. The main part of the tsunami energy was reflected by the Aleutian Islands and did not penetrate the Bering Sea. The maximum amplitudes of 50–60 cm occurred in Bristol Bay (Fig. 2a). In the west Bering Sea, the maximum amplitudes of 10–15 cm were in the Anastasia Bay. In neighboring Machevna Bay the amplitude reached 13 cm. The amplitudes decreased to 1–3 cm in the Bering Strait. Waves attenuated even more after passing the strait: the amplitudes were only up to 1 cm in Point Hope and even less (1 cm) on the coast of Wrangel Island. The central part of the Bering Sea, namely St. Lawerence Island and St. Matthew Island, was characterized by the wave amplitudes reaching 10 cm.

II. 1952 Kamchatka. The Great Kamchatka earthquake of 4 November 1952 was one of the largest earthquakes in the 20th century; it had the estimated magnitude of M_w = 9.0 (Johnson & Satake, 1999). The earthquake created a catastrophic tsunami. In the near-field region, the tsunami reached wave heights > 18 m and killed several thousand people in Severo-Kurilsk (Paramushir Island, Northern Kuril Islands) and southern Kamchatka, thus becoming the most devastating tsunami ever occurred in Russia (Gusiakov, 2014). The earthquake (52.75°N, 159.50°E) had a seismic moment, for different sources ranging from 180×10^{20} N·m to 350×10^{20} N·m or M_w = 8.8–9.0 (Johnson & Satake, 1999).

The tsunami source was taken from Johnson and Satake study (1999). They sought a slip distribution at 12 subfaults using inverse tsunami modeling technique and tide gauge observations in Alaska, Hawaii, Japan, and California. The optimum solution has an average *slip* of 3.2 m with a maximum of 11.4 m at the shallow water segment. The detailed source parameters are presented by (Johnson & Satake (1999). Using Okada's (1985) equations for each subfault, we computed the surface uplift distribution and then summarized all results gained into one composite tsunami source that is finally used in our modeling.
According to our modelled results (Fig. 2b), the tsunami waves generated by this earthquake came into the Bering Sea and had maximum amplitudes of 177 cm on the Russian coast at Machevna Bay. On the east (American) coast of the Bering Sea, the maximum wave amplitude was 66 cm in Norton Sound. Northwardly, the waves were becoming weaker: they were only of 10–18 cm in the Bering Strait region. Then in the Chukchi Sea, the simulated wave amplitudes were 7 cm in Kotzebue Sound, 3 cm at Point Hope and merely 1.8 cm on the coast of Wrangel Island. In the Bering Sea, at St. Matthew Island the simulated wave amplitude was 49 cm.

III. 1957 Andreanof Islands. This powerful tsunamigenic earthquake (51.50°N, 175.63°E) occurred on 9 March 1957 and had a magnitude of M_w = 8.6. The maximum tsunami wave amplitude was 32 m. It was recorded at Unalaska Island, the Aleutian Islands (Griswold et al., 2019). At Unimak, near Cape Scotch-Cap, the tsunami wave amplitude was about 22 m according to Lander (1996) or 12–15 m according to Soloviev & Go (1984). The north coast of Kauai Island (Hawaii) was hit by the waves that reached 16 m (Rabinovich et al., 2019). The tsunami spread throughout the Pacific Ocean and was recorded by more than 50 tide gauges

on the coast of the Hawaiian Islands, in Japan and in North and South America (NGDR/WDS tsunami database, NOAA 2022).

We used composite tsunami source reconstructed from subfault model of Johnson et al., 1994 and the Okada (1985) equations. Johnson et al. (1994) applied inverse tsunami modeling and non-negative least squares approach to get slip distribution from a set of 13 subfaults. The rupture zone was located along the Aleutian Ridge from the Semisopochnoi Island to Unalaska Island; the subfaults were located along the Aleutian Arc, so *dip* was 15°, the *strike* angle changed from 245° in the east to 270° in the west. The *rake* angle changed from pure dip-slip in the eastern end of the rupture zone to nearly equal components of dip-slip and strike-slip in the west. The resulting *slip* was from 0 to 8.6 m, which corresponds to a seismic moment of 88×10^{20} N m, that is M_w=8.6 (for more details, see Johnson et al., 1994).

The results of the 1957 Andreanof Islands tsunami modeling are shown in Fig. 2c. The energy flux of the tsunami was mainly directed towards the south. The highest simulated tsunami wave in the Bering Sea was 75 cm in Anastasia Bay on the Russian coast. The amplitudes were 49 cm and 45 cm at neighboring sites in Machevna Bay and Olyutorsky Gulf, respectively. The simulated wave amplitude was about 4 cm at Point Hope (Alaska) in the Chukchi Sea. The amplitudes of the computed tsunami waves were 3–6 cm in the Bering Strait; at Wrangel Island, the maximum amplitude was just 1.4 cm.

IV. 1960 Chile. The Great Chilean Earthquake of 22 May 1960 had a momentum magnitude of M_w = 9.5 and was the strongest earthquake ever instrumentally recorded; its epicenter was located at 38.37°S, 72.807°W, the depth of the hypocenter was 30 km (Kanamori, 1977). The rupture simulated by the variable slip planer model was approximately 900 km long, 130 km wide, with the maximum slip exceeding 40 m. It had the following angles: *Strike* = 7°, *Dip* = 20°, *Rake* = 80° (Barrientos & Ward, 1990; Moreno et al., 2009). The seismic moment release of this model was 2×10^{23} N·m. Our input of the 1960 tsunami source is based on the results of the recent seismic model of Moreno et al. (2009), who used coseismic coastal data and a finite element technique to reconstruct the seismic source of the Great Chilean 1960 earthquake. This source was used in the tsunami model of Rabinovich et al. (2011).

Figure 3a shows maximum computed Chilean tsunami amplitudes for the entire Pacific Ocean, the Bering and Chukchi seas. The tsunami energy flux was mainly directed northwestwards to the Marquesas, the Hawaiian Islands, the Philippines and Japan. These particular regions were catastrophically affected by the 1960 Chilean tsunami: The maximum observed far-field tsunami heights were 10.5 m on the Hawaiian Islands, 6–9 m on other Pacific islands and in Japan and 4–6 m in Russia (Berkman and Symons, 1960; Rabinovich et al., 2019).

According to our modeling results, the maximum tsunami wave amplitudes associated with the 1960 Chilean earthquake on the Russian coast of the Bering Sea were observed in Machevna Bay (up to 192 cm) and Korfa Bay/Olyutorsky Gulf (140 cm). On the east (Alaskan) coast of the sea, the amplitude of the tsunami wave was up to 135 cm in Bristol Bay. On St. Lawrence Island the wave amplitude was 57 cm. At the entrance into the Chukchi Sea, the wave amplitude values varied from 15 to 24 cm. At Point Hope, where the 1960 local habitats mentioned ice cracking and strong noise during the event, we estimated a wave

amplitude to be of only 3 cm. In Kotzebue Sound, it was a little more than 9 cm, while at Wrangel Island (the Chukchi Sea) it was 1.4 cm.

V. 1964 Alaska. On 27 March 1964, the Prince William Sound area of Alaska was struck by the largest earthquake ever recorded in North America and, in general, the strongest in the northern hemisphere. The megathrust earthquake with magnitude of M_w =9.2 generated the most destructive tsunami in Alaskan history. The tsunamis reached heights with 52 m runup at Shoup Bay (Lander, 1996). About 20 local landslide tsunamis were generated that had runups of up to 70 m (Lander 1996). The tectonic tsunami devastated many towns along the Gulf of Alaska, left severe damage in British Columbia, Hawaii, and along the western coast of the USA.

We used updated coseismic deformation model of Suleimani and Freymueller (2020) to simulate the event. This model is based on the results of Suito and Freymueller (2009) who developed a 3-D viscoelastic seismic source model in combination with an afterslip model. They used realistic geometry with a shallow-dipping elastic slab to describe the postseismic deformation initiated by the 1964 earthquake. The model of Suleimani et al. (2013) enabled us to evaluate the contribution of coseismic horizontal displacements into the initial tsunami wavefield. This additional component of the ocean surface uplift is caused by the horizontal displacement motion on the steep ocean bottom slope.
The energy flux of the 1964 Alaskan tsunami was mainly directed southeastward, to the west coasts of Canada (British Columbia) and the USA (Washington and Oregon) and then to the coasts of Peru and Chile (Fig. 3b). The highest simulated 1964 tsunami wave of 75 cm in the Bering Sea was identified in the Olyutorsky Gulf. It is remarkable that on the opposite (eastern) coast of the Bering Sea its amplitude had a comparable value of 65 cm. It appears that a branch of tsunami waves after penetrating the Bering Sea went around the Alaska Peninsula. On the coasts of the Bering Strait, the computed wave amplitudes were 10—15 cm. On the west coast, in the Kolyuchin Bay, there were 6-cm waves and about the same on the east, in Norton Bay. At Point Hope, the numerically simulated maximum wave amplitude was 2 cm and 1.3 cm at Wrangel Island. In the middle of the Bering Sea, on St. Matthew Island, the wave amplitude was 15 cm.

VI. 1965 Rat Islands. The strong earthquake (51.25 °N, 178.72°E) occurred on 4 February 1965 with M_w = 8.7. The earthquake generated a trans-Pacific tsunami, which hit the Aleutian Islands. At Amchitka and Attu Islands, the amplitude of the tsunami wave reached 1.5—2 m (Soloviev & Go, 1974; Lander, 1996). The height of the water rise was estimated to be 9—10 m, on the southern coast of Shemya Island (Soloviev & Go, 1974).

We used a slip distribution from (Johnson & Satake, 1996), which is based on the inverse tsunami modeling. The total source was considered as the sum of 14 sub-faults with slips ranging from 0 to 6 m. Each of these sub-faults had a spatial scale of 100·60 km with the following angles: *strike* = 290°, *rake* = 41.4°, *dip* = 18°. The seismic moment from the surface wave inversions was estimated from 66 to 140·10^{20} N·m.

The main direction of the Rat Islands tsunami energy flux was toward the southwest (Fig. 3c). In the Bering Sea, the maximum computed amplitude of the tsunami wave was 89 cm in Anastasia Bay and 64 cm at the Ozernoy Cape of Kamchatka) On St. Matthew and St. Lawrence Islands located in the open part of the sea, the wave amplitude was about 40 cm. On the Alaska coast, the amplitudes were smaller: 14—38 cm near

Kuskokwim River. In Bering Strait the amplitude was 15 cm. In the Chukchi Sea, the wave amplitude further decreases to 1.6 cm at Wrangel Island and to 5.2 cm at Point Hope.

VII. 2011 Tohoku-Oki. On 11 March 2011, a subduction megathrust earthquake with a moment magnitude M_w = 9.1 occurred 32 km below the ocean floor on the east coast of Honshu, Japan (Song et al., 2012). This earthquake and the following tsunami killed almost 20,000 people in Japan and caused widespread destruction. The Tohoku tsunami had a maximum runup of ~ 41 m in Japan (Aomori Prefecture); wave amplitudes were up to 2.5 m on the west coast of the USA and up to 2.3 m at Kuril Islands according to the tide gauge and runup field measurements (Mori et al., 2012; NGDC/WDS, 2022).

In this study, we used the finite-fault seismic source model constructed by Hayes (2011), who used 325 sub-faults, 25·20 km each, to estimate slip distribution. The low-angle nodal plane (*Dip* = 10°, *Strike* = 194.4°) was selected as the preferred fault plane, with dimensions of 650 km along the strike and 260 km across the strike. The seismic moment release of this model was $4.99 \cdot 10^{22}$ N·m which is somewhat smaller than the Global CMT solution ($5.59 \cdot 10^{22}$ N·m). The model was reformulated by Fine et al. (2013) based on Okada (1985) elastic equations and non-hydrostatic transformation to get a tsunami source. This tsunami source was used to model the wave energy decay and transformation in the Pacific Ocean (Fine et al. 2013).

The results of the 2011 Tohoku modeling are shown in Fig. 4a. The Tohoku tsunami energy spread mainly to the southeast, towards the South America (Peru and Chile). According to our simulations, the maximum amplitude of tsunami waves in the Bering Sea was observed in Machevna Bay (97 cm), at Commander Islands (91 cm) and in Olyutorsky Gulf (71 cm). In general, the waves are higher on the Russian coast comparing to the Alaskan coast, where wave amplitudes were below 39 cm. To the north, in the Bering Strait, the wave amplitudes decreased to 8—15 cm, and then further decrease in the Arctic; in the Chukchi Sea the largest 7cm high wave occurred in Kotzebue Sound, it was weaker at Point Hope (3 cm) and it had the amplitude of only 1.6 cm on the coast of Wrangel Island.

VIII. 2012 Haida Gwaii. A strong M_w=7.8 earthquake at 52.79°N, 132.101°W and a depth of 14 km occurred on 28 October 2012. This earthquake is likely associated with the relative motion across the Queen Charlotte fault system offshore of British Columbia, Canada. The earthquake was the second most powerful instrumentally recorded earthquake in Canadian history; it generated the largest local tsunami ever recorded on the coast of British Columbia. A field survey on the Pacific side of Haida Gwaii found up to 7.6 m above the tidal level at sites sheltered from the direct influence of incoming waves and up to 13 m in a small unsheltered inlet (Leonard & Bednarski, 2014; Fine et al., 2015). It generated waves of more than 1 m on the coast of the Hawaiian Islands (Fine et al., 2015).

We used the tsunami source model constructed by Fine et al. (2015) from the finite fault model of Hayes (USGS) to simulate the respective tsunami waves. According to our computations (Fig. 4b), the maximum waves were just below 14 cm on the west coast and 7—9 cm on the east coast of the Bering Sea. In the Chukchi Sea, the wave amplitudes were negligibly small, < 1 cm.

IX. 2017 Commander Islands. A strong earthquake (M_w 7.7) occurred on 17 July 2017 (54.44°N, 168.86°E, hypocenter depth 10 km) near the Commander Islands (Bering Island, Russia) as a result of transform

faulting on or near the plate boundary between the Pacific and North America plates in the Northwest Pacific Ocean. This earthquake was the largest earthquake instrumentally recorded in the Bering Sea basin since 1900. The earthquake generated a small tsunami; waves with amplitudes of up to 9 cm were observed at Shemia Island, Alaska (NGDR/WDS tsunami database, NOAA 2022). We used the parameters of the nodal plane from USGS: *Strike* = 305°, *Dip* = 86°, and *Rake* = 163° (USGS) to model the event. The size of the fault and the slip were estimated via scaling law of Wells and Coppersmith.
The results of the tsunami modeling are shown in Fig. 4c. At the coastal stations, the largest amplitude was in Olyutorskiy Gulf, 54 cm. At St. Matthew Island, the simulated amplitude was 14.8 cm, located in the direction of the main energy flux. Another local increase was in the neighborhood of the source on the coast of Kamchatka: 24 cm at the Ozernoy Cape. In the Bering Strait, the amplitude decreased to 0.4–0.5 cm and in the Chukchi Sea, the simulated tsunami waves were only 0.3 cm.

The tsunami waveforms (Fig. 5) differ significantly depending on the site location and parameters of the seismic source. The strongest earthquakes (Kamchatka, Chile, Alaska, Tohoku) generated waves with a noticeable contribution of low-frequency components (Fig. 5). Weaker earthquakes, which sources were located along the Aleutian Ridge, generated higher-frequency sea level oscillations. This is apparently due to the smaller corresponding source sizes and their extension along with the Aleutian Islands; as a result, relatively high-frequency tsunami waves were directed towards the Bering Sea. Various coastal sites have different frequency-selective properties. This significantly influenced the tsunami waveforms in individual gulfs, bays, and inlets. Thus, in Korfa and Bristol bays, the arriving tsunami waves caused significant intensification of their natural (*eigen*) oscillations with typical periods of 20–25 minutes for most events. In Bristol Bay and Kresta Bay, tsunami waveforms have a longer prevailing period (Fig. 5). The highest tsunami waves in the Bering Sea were caused by the 1960 Chile earthquake. In Korfa Bay, the trough-to-creast heights of generated sea-level oscillations reached 2 m and during 10 hours had a steady monochromatic character with a period of ~ 1.5 hours (Fig. 5).

4. Penetration Of Tsunami Waves Through Straits

One of the important problems in the tsunami research is penetration of far-field tsunamis from the Pacific Ocean into the Bering Sea through the multiple straits of the Aleutian Islands. The effect of tsunami attenuation by straits was examined by Soloviev and Kulikov (1987) for tsunamis of 13 and 20 October 1963 incoming into the Sea of Okhotsk from the Pacific Ocean through the straits of the Kuril Islands. The authors indicated that the wave amplitude decreased by a factor of 2–2.5 after passing through these straits. Soloviev and Kulikov (1987) assumed that the amount of diffracted wave energy was determined mainly by the width of the deep-ocean straits. The ratio of their total width to the entire length of the island arc was about 25%. This number is in agreement with the transmittance coefficient: $k = 0.21$. Such a simple estimate is approximate and does not reflect all possible effects that arise when a wave passes through a ridge of islands. Depending on the ratio of the wavelength to the straight width, the amount of diffracted wave energy can vary greatly. For typical tsunami waves, wavelength are usually exceeds the width of the strait, and in that case the strait is work as low-pass filter that transmit long waves and attenuate short waves. To understand the low pass filter effect, the electric analogy of the wave transformations could be used. According to Miles (1971), the straits in equivalent-circuit analysis is replaced to the coil. The inductive

reactance of the coil increases with increase in frequency, thus the wave with higher frequency will be stronger attenuated while passing the strait.

To evaluate the effect of the attenuation of the tsunami waves passing through the Aleutian chain of islands, in our model calculations we placed reference points directly in front of the straits in the Pacific Ocean and inside the Bering Sea waters at a distance of about 250 km from the strait exits. Table 2 shows the maximum tsunami amplitudes for two major events: the 1960 Chile tsunami (Fig. 6a) and the 2011 Tohoku tsunami (Fig. 6b). Similar estimations were done for the Bering Strait. It turned out that the typical attenuation coefficient for the straits of the Aleutian ridge is 0.6–0.8 (0.75 on average), while the coefficient of tsunami attenuation upon the transition from the Bering Sea to the Arctic Ocean is ~ 0.25. We can conclude that tsunami penetration into the Arctic Ocean from remote sources in the Pacific Ocean is highly unlikely. Even for such powerful events as the 1960 Chile tsunami, the amplitudes of simulated waves in the Chukchi Sea do not exceed a few centimeters. It appears that tsunamis generated directly in the Arctic Ocean are the main danger for this ocean.

Table 2
Tsunami amplitudes (cm) outside and inside the straits, and the ratio: outside/inside.

Strait	LAT	LON	1960 Chile			2011 Tohoku		
			Outside	Inside	Ratio	Outside	Inside	Ratio
Unimak	54.33	194.91	17.0	23.0	0.7	6.7	14.9	0.4
Chuginadak I.—Nikolskiy I.	52.92	190.70	15.1	13.3	1.1	8.3	9.7	0.9
Seguam Island—Amukta I.	52.36	188.09	13.8	8.5	1.6	10.8	9.2	1.2
Tagalak I.—Oglodak I.	51.99	184.52	13.6	7.0	2.0	14.0	5.3	2.6
Amchitka I.—Amatignak I.	51.51	179.98	11.4	10.8	1.1	20.6	17.6	1.2
Near Islands—Rat Isl.	52.32	174.45	12.3	9.8	1.3	21.1	8.7	2.4
The Commander Isl.— Attu I.	53.48	170.28	13.2	11.8	1.1	18.0	7.3	2.5
Kamchatka Strait	55.86	164.34	16.8	13.2	1.3	8.7	5.6	1.6
Bering Strait	65.97	190.58	4.9	1.7	3.0	4.3	1.1	3.9
	65.68	191.58	6.6	2.0	3.3	4.8	1.4	3.5
Mean					1.6			2.0

5. Discussions And Conclusions

Thus, the problem of tsunamis in the Arctic region and adjacent seas, in particular in the Bering and Chukchi seas, as well as the penetration of trans-oceanic tsunamis there, is poorly understood and relevant, especially in connection with the increasing development of the region. In this study, the main target was to analyze the most powerful trans-oceanic Pacific tsunamis: how do they penetrate the Arctic region? Using numerical

modeling, we reproduced the strongest tsunamis of the Pacific Ocean of the 20th and 21st centuries. Also, we considered the maximum inner earthquakes to examine would they cause noticeable tsunamis in this region and what would be their characteristics?

Summarizing all our findings, we conclude that the most dangerous for the Bering Sea of all examined tsunami events was the 1960 Chilean tsunami. According to our simulations, it created a 192-cm tsunami wave amplitude in this sea (Table 3). Regarding the other examined events, the second most dangerous event was the 1952 Kamchatka tsunami. It is natural, taking into account its magnitude (M_w 9.0) and closeness to the Bering Sea basin. The 1964 Great Alaska earthquake did not produce any significant tsunami waves in the Bering Sea, because that basin is sheltered from the incoming waves by the Alaska Peninsula.

However, for specific sites the maximum simulated wave amplitudes were associated nor with 1960 Chile, neither with the 1952 Kamchatka tsunamis. To be more precise, the largest tsunami waves that occurred at Point Hope (~ 5 cm) were produced by the 1965 Rat Islands earthquake. It appears that this was due to the strike orientation (305°) when the main flux from the source was directed into the strait. For the same reason (*Strike* = 290°) the relatively weak 2017 Commander Islands earthquake generated higher amplitude waves for the St. Lawrence Island more distant from the source than for closer St. Matthew Island. We may assume that the source strike has to be in the range of 290–300° for the most effective penetration of tsunami waves into the Chukchi Sea. Our numerical experiments also demonstrate the tsunami energy concentration in particular coastal bays and inlets. Typically, in these bays the tsunami amplitude is significantly higher than on the open coast due to some local resonant harbour effects.

Another important point is that in all studied cases, the west coast of the Bering Sea was more vulnerable to tsunami waves, independently of the source orientation, location and off-source distance. All local maxima for both west and east Bering Sea coasts were associated with semi-closed inner basins: Machevna Bay, Bristol Bay, Anastasia Bay, etc. Moreover, the most powerful distant earthquakes (1960 Chile, 2011 Tohoku, and 1952 Kamchatka) induced the highest tsunami amplitudes in these specific, relatively large bays. In contrast, the closer and relatively weaker earthquakes (1957 Andreanof and 1965 Rat Islands) produced larger oscillations in smaller bays, such as Anastasia Bay. It appears that this was because the great earthquakes had relatively large source areas and, consequently, longer dominant periods of generated tsunami waves, while weaker tsunamigenic earthquakes had smaller sources and shorter prevailing periods. Correspondingly, the great tsunamis (like 1952, 1960, and 2011) were resonantly amplified in larger bays, while weaker events (1957 and 1965) in smaller bays.

Table 3
The computed maximum tsunami amplitudes (in cm) at various locations in the Bering and Chukchi Seas.

Earthquake	M_w	Bering Sea		Kotzebue	Point Hope	Wrangel
		West coast	East coast			
1946 Aleutian	8.6	60	60	3	3	1
1952 Kamchatka	9.0	178	66	7	3	2
1957 Andreanof Islands	8.6	61	65	4	4	2
1960 Chile	9.5	95	83	9	5	2
1964 Alaska	9.2	74	65	6	2	1
1965 Rat Islands	8.7	89	38	4	5	1
2011 Tohoku	9.1	97	42	7	3	2
2012 Haida Gwaii	7.8	14	9	< 1	< 1	< 1
2017 Commander Islands	7.7	54	4	< 1	< 1	< 1

As the result, we came to a conclusion that tsunami waves formed by the strongest distant earthquakes could have reached 1–1.5 m in the largest bays of the Bering Sea (for example, in Machevna and Bristol Bay). Significant earthquakes are often accompanied by underwater landslide failures, which could locally increase the height of the generated tsunami waves greatly. Recent earthquakes, like the one in Palu Bay (2018, Sulawesi Island, Indonesia) had a magnitude of M_w 7.5 and triggered a local landslide that produced catastrophic tsunami waves up to 9 m high, leading to a significant number of casualties among civilians (Omira et al., 2019). A similar effect could potentially occur in the Bering and Chukchi seas.

The interest in studying tsunamis in the Bering and Chukchi seas is stimulated by local activities such as shipping, fishing, and the development of oil and gas fields in these regions. It is important to emphasize that in 2020–2021 four significant earthquakes with $M_w \geq 7.5$ occurred near the Aleutian Islands: 25 March 2020 (M_w 7.5), 22 July 2020 (M_w 7.8), 19 October 2020 (M_w 7.8), and 29 July 2021 (M_w 8.2) (USGS). These seismic events did not cause large tsunamis, but they demonstrated that the seismic potential of this region is very high. A much more powerful tsunamigenic earthquake is quite possible here. This is one of the reasons why the Bering Sea region should be prepared for the tsunami hazard. The most dangerous are tsunamigenic seismic sources located on the contact border between the Pacific and North American lithospheric plates along the Aleutian Islands and on possible tsunamis from underwater landslides (Sawyer et al., 2017; Tsukanov et al., 2019).

Declarations

Acknowledgments

This study is dedicated to the memory of our friend and colleague, Dr. Evgueni Kulikov (27.01.1950–21.11.2020), who suddenly passed away. Evgueni took an active part in setting this study, generously helped in this research through his discussions, mathematical insight and sense of humor. The authors gratefully acknowledge Alexander Rabinovich and Richard Thomson from the Institute of Ocean Sciences (Sidney, BC, Canada) for valuable comments and suggestions.

Funding

This study was supported by the Russian State Assignment of IORAS FMWE-2021-0004 and by the RFBR grant #17-05-41144.

Author Contributions Statement

A.M. wrote the main manuscript text, made numerical simulations, analysis, visualization. I.M. gave the principal idea of the research, and prepared data from external sources. I.F. configured the model, and prepared input seismic data. E.K. helped with developping of this study and set the experiment with straits, described and interpreted the results. O.Y. plotted and updated figures. All authors reviewed the manuscript and improoved the text.

Conflict of interest

We declare that the authors have no competing interests as defined by Springer, or other interests that might be perceived to influence the results and/or discussion reported in this paper.

The results/data/figures in this manuscript have not been published elsewhere, nor are they under consideration (from you or one of your Contributing Authors) by another publisher.

References

1. Barrientos, S. E., & Ward, S. N. (1990). The 1960 Chile earthquake: inversion for slip distribution from surface deformation. Geophysical Journal International, *103*(3), 589–598. https://doi.org/10.1111/j.1365-246X.1990.tb05673.x
2. Berkman, S. C., & Symons, J. M. (1960). The tsunami of May 22, 1960 as recorded at tide gauge stations. US Department of Commerce, Coast and Geodetic Survey, Washington, D.C., 79 pp.
3. Bourgeois, J., Pinegina, T. K., Ponomareva, V., & Zaretskaia, N. (2006). Holocene tsunamis in the southwestern Bering Sea, Russian Far East, and their tectonic implications. Bulletin of the Geological Society of America, *118*(3–4), 449–463. https://doi.org/10.1130/B25726.1
4. Dudley, W. C., & Lee, M. (1998). Tsunami! *University of Hawaii Press*. https://doi.org/10.1515/9780824865306
5. Fine, I. V., Kulikov, E. A., & Cherniawsky, J. Y. (2013). Japan's 2011 tsunami: Characteristics of wave propagation from observations and numerical modelling. Pure and Applied Geophysics, *170*(6–8), 1295–1307. https://doi.org/10.1007/s00024-012-0555-8

6. Fine, I. V., Cherniawsky, J. Y., Thomson, R. E., Rabinovich, A. B., & Krassovski, M. V. (2015). Observations and Numerical Modeling of the 2012 Haida Gwaii Tsunami off the Coast of British Columbia. Pure and Applied Geophysics, *172*(3–4), 699–718. https://doi.org/10.1007/s00024-014-1012-7
7. Gordeev, E. I., Pinegina, T. K., Lander, A. V., & Kozhurin, A. I. (2015). Beringia: Seismic hazard and fundamental problems of geotectonics. Izvestiya, Physics of the Solid Earth, *51*(4), 512–521. https://doi.org/10.1134/S1069351315030039
8. Griswold, F. R., MacInnes, B. T., & Higman, B. (2019). Tsunami-based evidence for large eastern Aleutian slip during the 1957 earthquake. Quaternary Research, *91*(3), 1045–1058. https://doi.org/10.1017/qua.2018.39
9. Gusiakov, V. K. (2014). Strongest tsunamis in the World Ocean and the problem of marine coastal security *Izvestiya, Atmospheric and Oceanic Physics, 50*(5), 435–444. https://doi.org/10.1134/S0001433814050041
10. Gusiakov, V.K., Dunbar, P.K., & Arcos, N. (2019). Twenty-Five Years (1992–2016) of Global Tsunamis: Statistical and Analytical Overview. Pure Appl. Geophys. *176*, 2795–2807. https://doi.org/10.1007/s00024-019-02113-7
11. Hayes, G. (2011). Rapid source characterization of the 2011 M_W 9.0 off the Pacific coast of Tohoku earthquake, Earth Planets Space, *63*, 529–534. https://doi.org/10.5047/eps.2011.05.012
12. Imamura, F. (1996). Review of tsunami simulation with a finite difference method. In: *Long-Wave Run-up Models*, (Eds. by H. Yeah, P. Liu, and C. Synolakis), World Scientific, Singapore, 1996, 25–42.
13. Johnson, J. M., & Satake, K. (1996). The 1965 Rat Islands earthquake: A critical comparison of seismic and tsunami wave inversions. Bulletin of the Seismological Society of America, *86*(5), 1229–1237. https://doi.org/10.1785/BSSA0860051229
14. Johnson, J. M., & Satake, K. Estimation of seismic moment and slip distribution of the April 1, 1946, Aleutian tsunami earthquake (1997). Journal of Geophysical Research: Solid Earth, *102*(B6), 11765–11774. https://doi.org/10.1029/97JB00274
15. Johnson, J. M., & Satake, K. (1999). Asperity distribution of the 1952 Great Kamchatka earthquake and its relation to future earthquake potential in Kamchatka. Pure and Applied Geophysics, *154*, 541–553. https://doi.org/10.1007/s000240050243
16. Johnson, J. M., Tanioka, Y., Ruff, L. J., Satake, K., Kanamori, H., & Sykes, L. R. (1994). The 1957 great Aleutian earthquake. Pure and Applied Geophysics, *142*(1), 3–28. https://doi.org/10.1007/BF00875966.
17. Kanamori, H. (1977). The energy release in great earthquakes. Journal of Geophysical Research, *82*(20), 2981–2987. https://doi.org/10.1029/JB082i020p02981
18. Kulikov, E. A., Ivashchenko, A. I., Medvedev, I. P., Fine, I. V., & Yakovenko, O. I. (2019a). Tsunami hazards for the Arctic coast of Russia. Part 1. The catalogue of probable tsunamigenic earthquakes. Georisk World, *13*(2), 18–32, https://doi.org/10.25296/1997-8669-2019-13-2-18-32 (in Russian)
19. Kulikov, E. A., Ivashchenko, A. I., Medvedev, I. P., Fine, I. V., & Yakovenko, O. I. (2019b). Tsunami hazards for the Arctic coast of Russia. Part 2. Numerical tsunami modelling. Georisk World, *13*(3), 6–17, https://doi.org/10.25296/1997-8669-2019-13-3-6-17 (in Russian)

20. Lander, J. F. (1996). *Tsunamis Affecting Alaska, 31, 1737–1996*. US Department of Commerce, National Oceanic and Atmospheric Administration, National Geophysical Data Center, 195 p.
21. Leonard, L. J., & Bednarski, J. M. (2014), Field survey following the 27 October 2012 Haida Gwaii tsunami, Pure and Applied Geophysics, *171*, 3467–3482. https://doi.org/10.1007/s00024-014-0792-0
22. Mackey, K. G., Fujita, K., Gunbina, L. V., Kovalev, V. N., Imaev, V. S., Koz'min, B. M., & Imaeva, L. P. (1997). Seismicity of the Bering Strait region: Evidence for a Bering block. Geology, *25*(11), 979–982. https://doi.org/10.1130/0091-7613(1997)025<0979:SOTBSR>2.3.CO;2
23. Miles, J. W. (1971). Resonant response of harbours: equivalent-circuit analysis. Journal of Fluid Mechanics, *46*(2), 245–265 https://doi.org/10.1017/S002211207100051X
24. Moreno, M. S., Bolte, J., Klotz, J., & Melnick, D. (2009). Impact of megathrust geometry on inversion of coseismic slip from geodetic data: Application to the 1960 Chile earthquake. Geophysical Research Letters, *36*(16). https://doi.org/10.1029/2009GL039276
25. Mori, N., Takahashi, T., & The 2011 Tohoku Earthquake Tsunami Joint Survey Group (2012). Nationwide post event survey and analysis of the 2011 Tohoku Earthquake Tsunami. Coastal Engineering Journal, JSCE, *54*(1), 1250001. https://doi.org/10.1142/S0578563412500015
26. NGDC/WDS (National Geophysical Data Center / World Data Service): Global Historical Tsunami Database. NCEI, NOAA. Boulder, CO, USA (2022). https://doi.org/10.7289/V5PN93H7
27. Okada, Y. (1985). Surface deformation due to shear and tensile faults in a half-space. Bulletin of the seismological society of America, *75*(4), 1135–1154.
28. Okal, E. A., Plafker, G., Synolakis, C. E., & Borrero, J. C. (2003) Near-field survey of the 1946 Aleutian tsunami on Unimak and Sanak islands. Bulletin of the Seismological Society of America, *93*(3), 1226–1234. https://doi.org/10.1785/0120020198
29. Omira, R., Dogan, G. G., Hidayat, R., Husrin, S., Prasetya, G., Annunziato, A., & Zaytsev, A. (2019). The September 28th, 2018, Tsunami In Palu-Sulawesi, Indonesia: A post-event field survey. Pure and Applied Geophysics, *176*(4), 1379–1395. https://doi.org/10.1007/s00024-019-02145-z
30. Pinegina, T. K., Kozhurin, A. I., & Ponomareva, V. V. (2014). Active tectonics and geomorphology of the Kamchatsky Bay coast in Kamchatka. Russian Journal of Pacific Geology, *8*(1), 65–76. https://doi.org/10.1134/S1819714014010047
31. Pinegina, T. K., Bazanova, L. I., Zelenin, E. A., Bourgeois, J., Kozhurin, A. I., Medvedev, I. P., & Vydrin, D. S. (2018). Holocene Tsunamis in Avachinsky Bay, Kamchatka, Russia. Pure and Applied Geophysics, *175*(4), 1485–1506. https://doi.org/10.1007/s00024-018-1830-0
32. Pinegina, T. K., Bourgeois, J., Bazanova, L. I., Zelenin, E. A., Krasheninnikov, S. P., & Portnyagin, M. V. (2020). Coseismic coastal subsidence associated with unusually wide rupture of prehistoric earthquakes on the Kamchatka subduction zone: A record in buried erosional scarps and tsunami deposits. Quaternary Science Reviews, *233*, 106171. https://doi.org/10.1016/j.quascirev.2020.106171
33. Rabinovich, A. B., Thomson, R. E., & Fine, I. V. (2013). The 2010 Chilean tsunami off the west coast of Canada and the northwest coast of the United States. Pure and Applied Geophysics, *170*, 1529–1565. https://doi.org/10.1007/s00024-012-0541-1

34. Rabinovich, A. B., Thomson, R. E., Krassovski, M. V., Stephenson, F. E., & Sinnott, D. C. (2019). Five great tsunamis of the 20th century as recorded on the coast of British Columbia. Pure and Applied Geophysics, *176*(7), 2887–2924. https://doi.org/10.1007/s00024-019-02133-3
35. Sawyer, D. E., Reece, R. S., Gulick, S. P., & Lenz, B. L. (2017). Submarine landslide and tsunami hazards offshore southern Alaska: Seismic strengthening versus rapid sedimentation. Geophysical Research Letters, *44*(16), 8435–8442. https://doi.org/10.1002/2017GL074537
36. Soloviev, S. L., & Kulikov, E. A. (1987). Restoring the Parameters for the Origin of Tsunamis from the Spectral Characteristics of Waves at the Shore. Atmospheric and Oceanic Physics, *23*(1), 66–71.
37. Soloviev, S. L., & Go, C. N. (1974). A catalogue of tsunamis on the western shore of the Pacific Ocean (p. 308). Moscow: “Nauka” Publishing House. (in Russian; English translation by the Canadian Institute for Scientific and Technical Information, No.5077, National Research Council, Ottawa, Canada, 1984, 439 pp.).
38. Song, Y. T., Fukumori, I., Shum, C. K., & Yi, Y. (2012). Merging tsunamis of the 2011 Tohoku-Oki earthquake detected over the open ocean. Geophysical Research Letters, *39*(5). https://doi.org/10.1029/2011GL050767
39. Suito, H., & Freymueller, J. T. (2009). A viscoelastic and afterslip postseismic deformation model for the 1964 Alaska earthquake. Journal of Geophysical Research: Solid Earth, *114*(B11). https://doi.org/10.1029/2008JB005954
40. Suleimani, E. N., & Freymueller, J. T. (2020). Near-field modeling of the 1964 Alaska tsunami: The role of splay faults and horizontal displacements. Journal of Geophysical Research: Solid Earth, 125, e2020JB019620. https://doi.org/10.1029/2020JB019620
41. Tsukanov, N. V., Dozorova, K. A., & Gaedicke, C. (2019). Specific features of the upper sedimentary cover and slump structures in the NW Pacific and the Bering Sea based on seismosacoustic profiling data. Bulletin of Kamchatka Regional Association "Educational-Scientific Center. Earth Sciences, *1*, 73–84. https://doi.org/10.31431/1816-5524-2019-1-41-73-84
42. USGS, United States Geological Survey https://earthquake.usgs.gov/earthquakes/search/
43. Van Dorn, W. G. (1987). Tide gage response to tsunamis. Part II: Other oceans and smaller seas, Journal of Physical Oceanography, *17*, 1507–1516. https://doi.org/10.1175/1520-0485(1987)017<1507:TGRTTP>2.0.CO;2
44. Wells, D. L., & Coppersmith, K. J. (1994). New empirical relationships among magnitude, rupture length, rupture width, rupture area, and surface displacement. Bulletin of the Seismological Society of America, *84*(4), 974–1002. https://doi.org/10.1785/BSSA0840040974

Figures

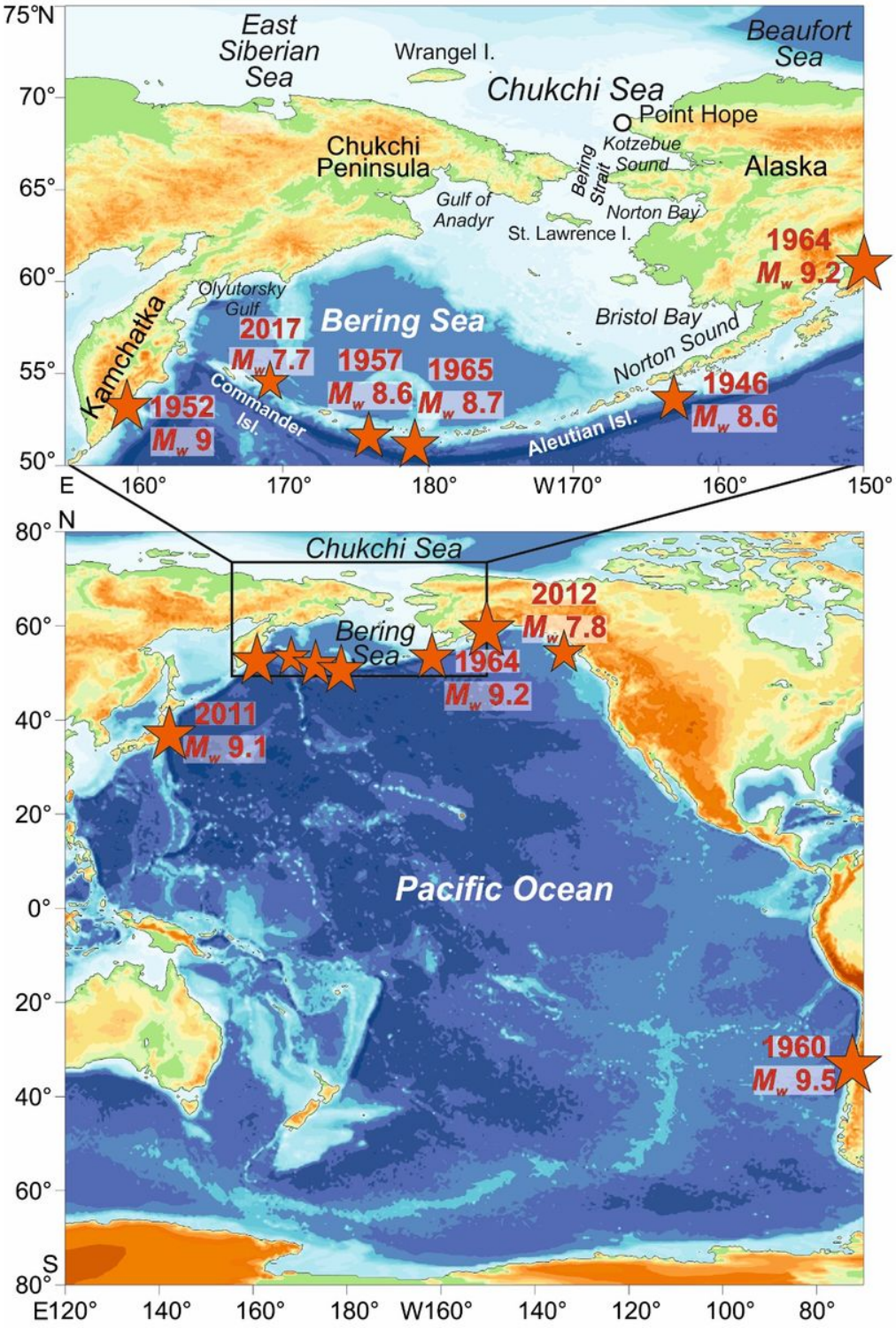

Figure 1

Map of the Pacific Ocean and adjacent Arctic Ocean showing the epicenters of the earthquakes (red stars).

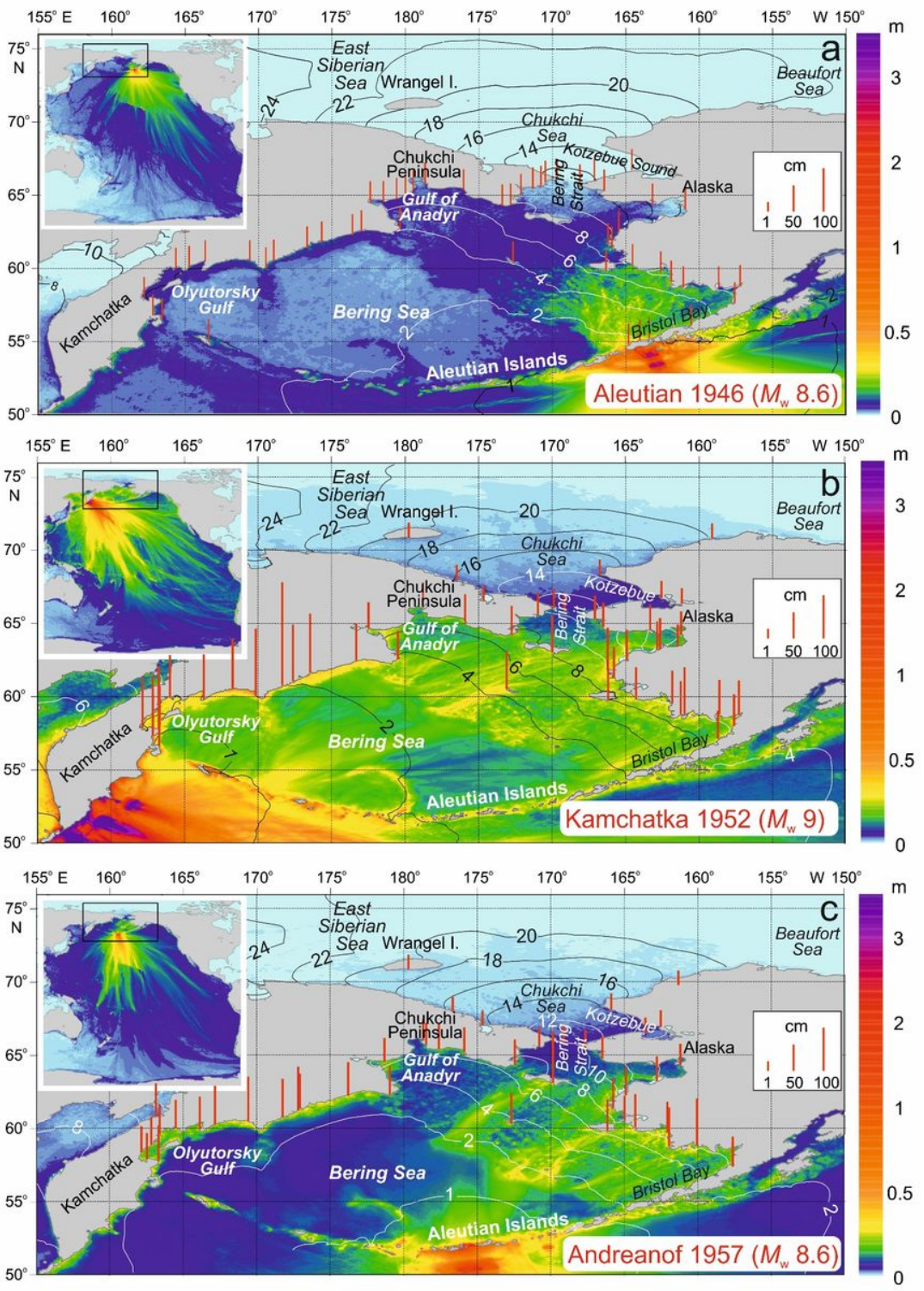

Figure 2

Maximum tsunami wave amplitudes produced by (a) the 1946 Aleutian, (b) the 1952 Kamchatka, and (c) the 1957 Andreanof Islands earthquakes. White and grey lines show the tsunami arrival time (in hours).

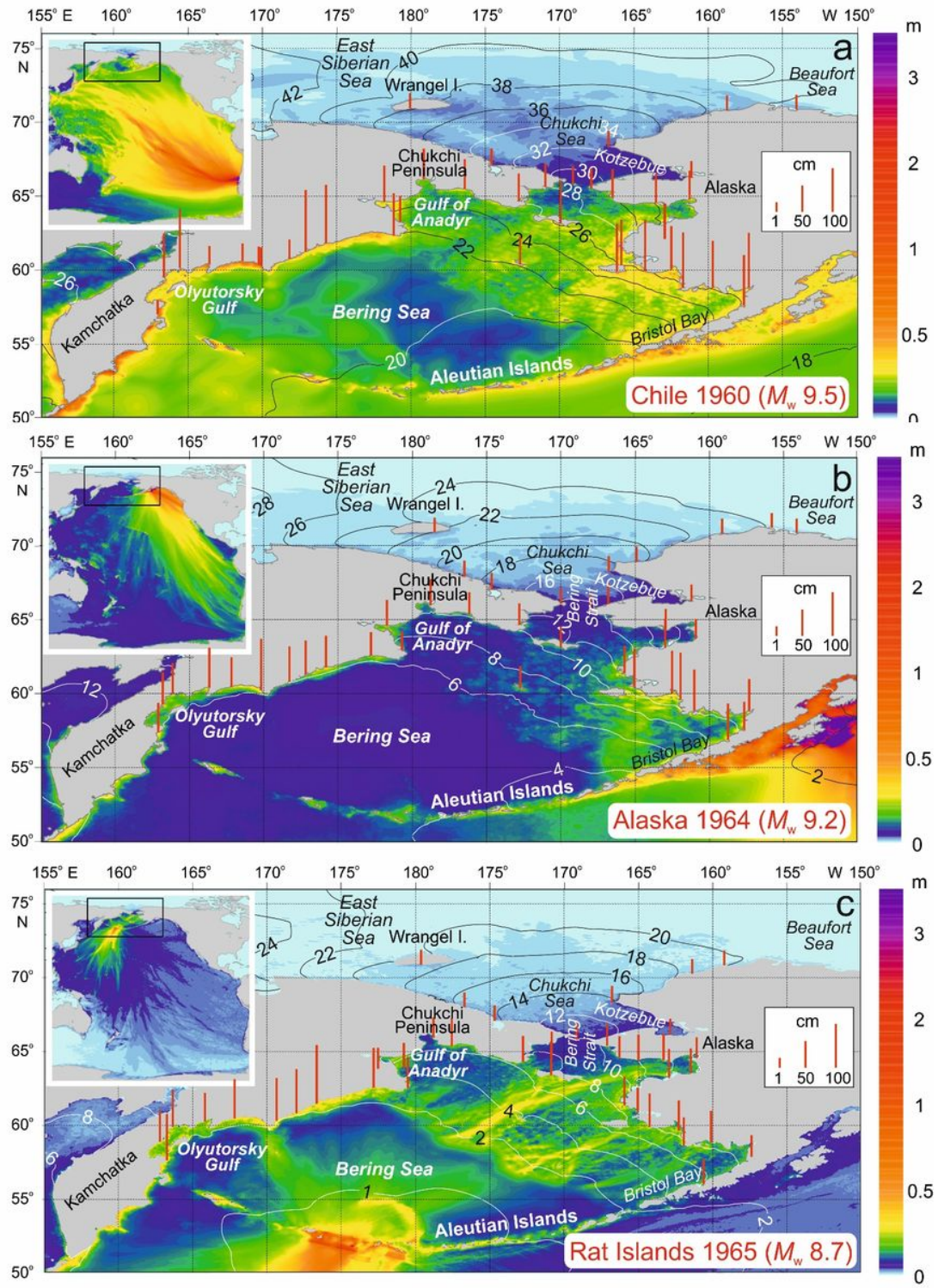

Figure 3

Maximum tsunami wave amplitudes produced by (a) the 1960 Great Chilean, (b) the 1964 Alaska, and (c) the 1965 Rat Islands earthquakes. White and grey lines show the tsunami arrival time (in hours).

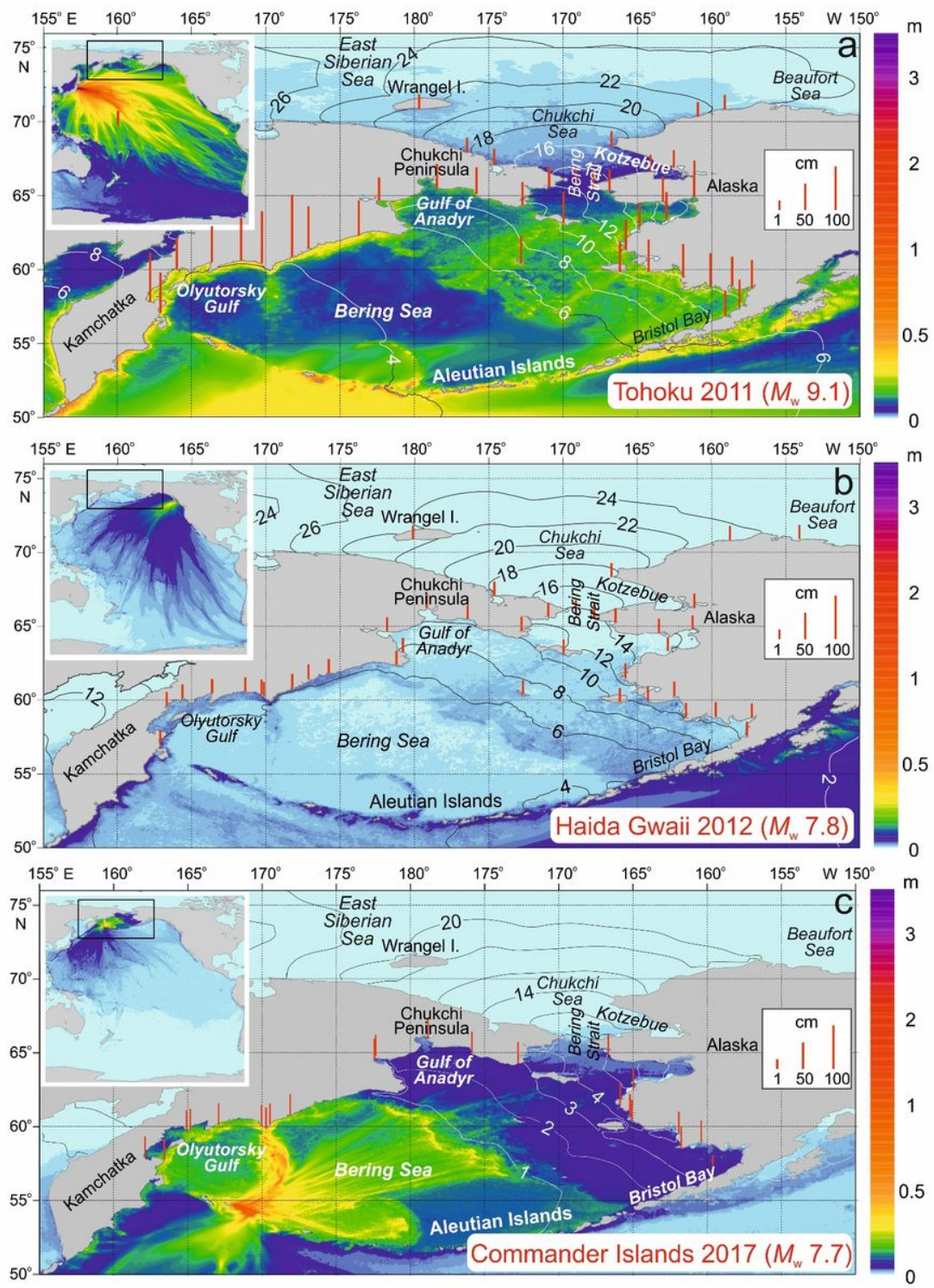

Figure 4

Maximum tsunami wave amplitudes produced by (a) the 2011 Tohoku, (b) the 2012 Haida Gwaii, and (c) the 2017 Commander Islands earthquakes. White and grey lines show the tsunami arrival time (in hours).

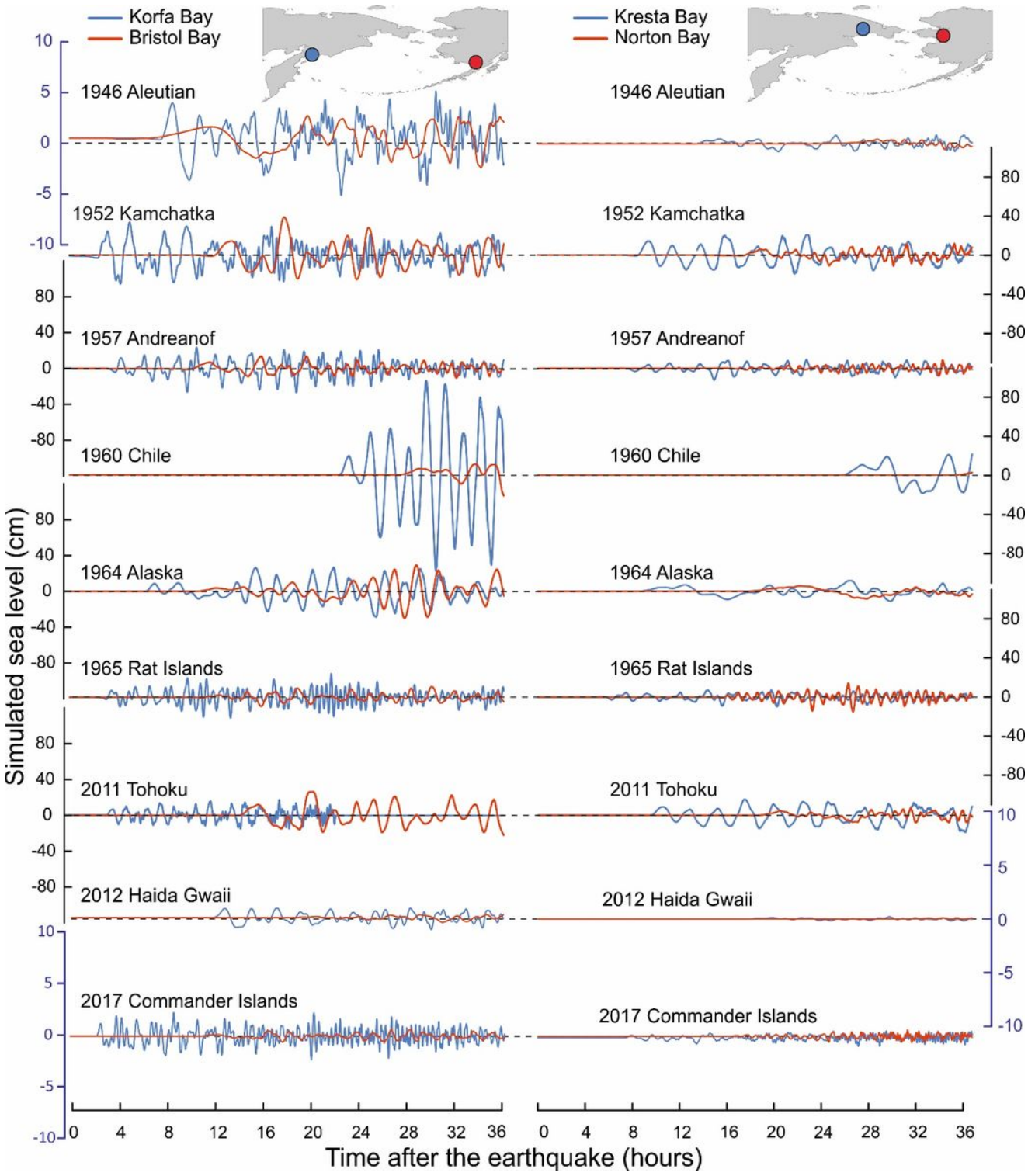

Figure 5

Simulated tsunami waveforms for nine earthquakes at four coastal sites

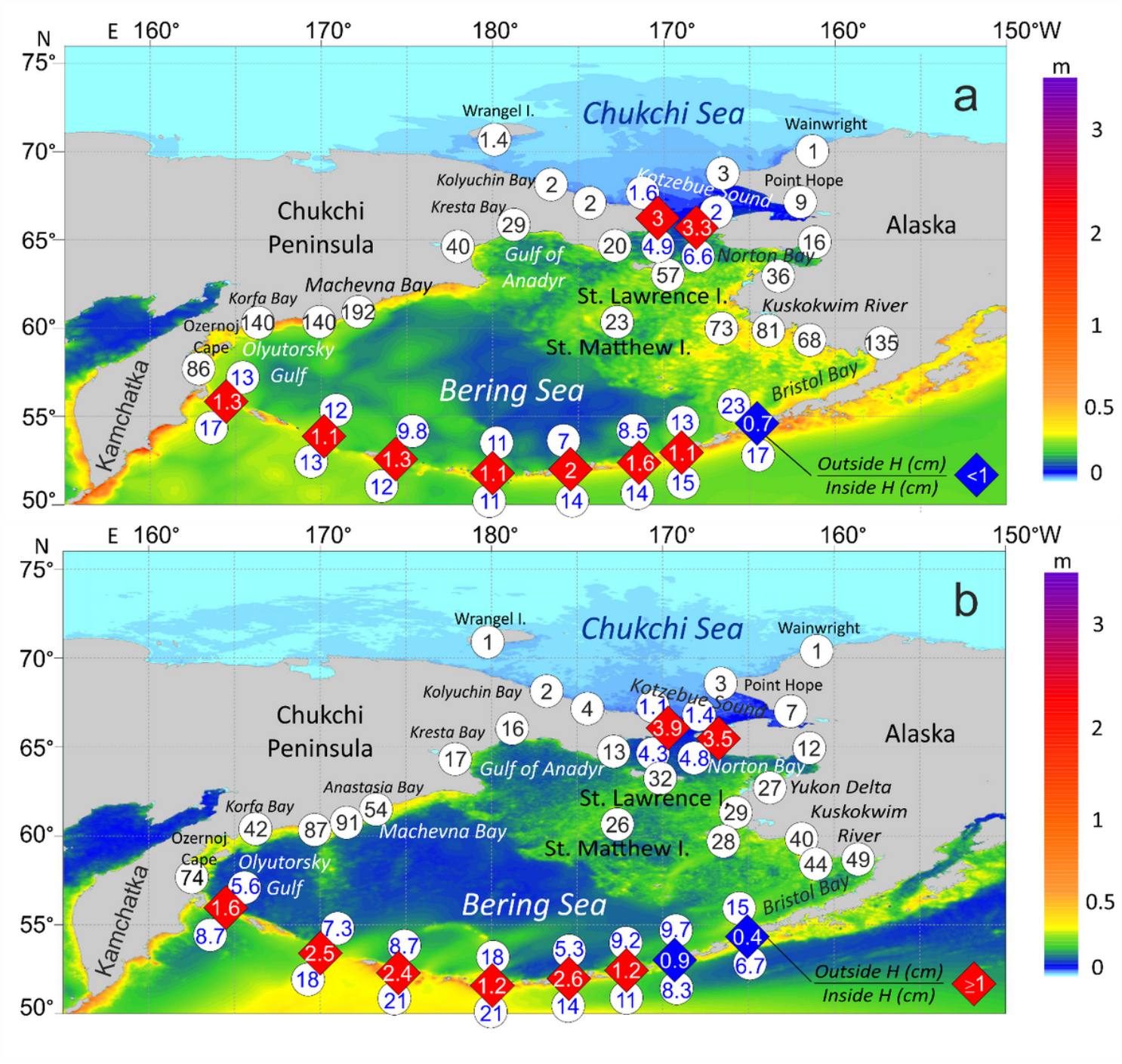

Figure 6

The maximum computed tsunami wave amplitudes in the Pacific Ocean and in the Bering Sea for (a) 1960 Chile and (b) 2011 Tohoku tsunamis. The wave amplitudes (in cm, inside white circles) are indicated by blue (for straits only) and black numbers. The amplitude ratios between the outside and inside amplitude values are denoted by numbers within red (attenuated amplitude) and blue (amplified amplitude) rhombuses.